Atmospheric Environment 209 (2019) 112–124

Contents lists available at ScienceDirect

Atmospheric Environment

journal homepage: www.elsevier.com/locate/atmosenv

Sensitivity of isoprene emissions to drought over south-eastern Australia: Integrating models and satellite observations of soil moisture

Kathryn M. Emmerson[a,*], Paul I. Palmer[b], Marcus Thatcher[a], Vanessa Haverd[c], Alex B. Guenther[d]

[a] CSIRO Oceans and Atmosphere, PMB1, Aspendale, VIC 3195, Australia
[b] School of GeoSciences, University of Edinburgh, Edinburgh, EH9 3JW, UK
[c] CSIRO Oceans and Atmosphere, Black Mountain, Canberra, ACT 2601, Australia
[d] Department of Earth System Science, University of California, Irvine, 92697, USA

GRAPHICAL ABSTRACT

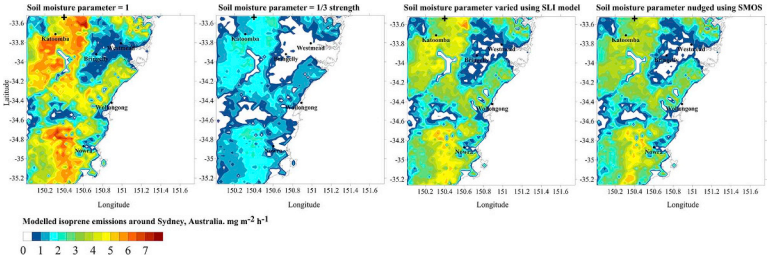

ARTICLE INFO

Keywords:
Isoprene emissions
Drought
Soil moisture
SMOS

ABSTRACT

South-east Australia, characterized by arid and semi-arid climate, has experienced large-scale rainfall reductions in recent decades. Larger temporal and spatial drought conditions are predicted in future. The temperate south east coastal zone is characterized by dense forests of Eucalyptus. Drought conditions have implications for the functioning of these indigenous ecosystems, and for emissions of reactive gases that are upwind of major metropolitan regions along the eastern coast. Here, we focus on the impact of drought on the emission of isoprene, a volatile organic compound emitted by a range of trees and shrubs. Previous model calculations grossly overestimate observations of the isoprene mixing ratio, potentially due to overestimated emission factors for native vegetation, but could also be due to drought-induced isoprene emission reductions. We develop the implementation of the Model of Emissions of Gases and Aerosols from Nature (MEGAN) within the CSIRO Chemical Transport Model to include a parameterization of drought using soil moisture. We test this parameterization using two approaches. First, we drive MEGAN using soil moisture fields from two Australian land surface models achieving reductions in isoprene emissions of 24–52% during summer. Second, we use a simple statistical approach to nudge model soil moisture towards satellite observations from the Soil Moisture and Ocean Salinity (SMOS) instrument. This work is the first application of SMOS towards isoprene emission modelling, providing a constraint on surface soil moisture which extends to global scales. Applying these soil moisture approaches, domain average isoprene emissions reduce by 38–58% in summer. Using these results, errors in basal emissions are likely in the region of 40%. Comparison of modelled soil moisture to observations using root density weighted averages across depths of 4 m showed minor differences of up to 0.04 $m^3 m^{-3}$. We find that the choice of land surface model used in the SMOS assimilations has a greater impact on isoprene emissions than adjusting either the nudging strength or the number of soil levels these satellite data may influence. However there are only small differences of 3% when using hourly or 24-hourly soil moisture input data to drive the emission calculations, suggesting that the lower temporal availability of satellite data does not reduce model quality. As

* Corresponding author.
E-mail address: kathryn.emmerson@csiro.au (K.M. Emmerson).

https://doi.org/10.1016/j.atmosenv.2019.04.038
Received 11 September 2018; Received in revised form 15 April 2019; Accepted 17 April 2019
Available online 18 April 2019

the spatial resolution of satellite observations of atmospheric composition and land surface properties begin to approach the resolution of regulatory air quality models, we anticipate that these data will improve model predictive skills further.

1. Introduction

Biogenic volatile organic compounds (BVOCs) are emitted by terrestrial and marine ecosystems and represent $\sim$1000 Tg C yr^{-1} to the atmosphere (Guenther et al., 2012). On a global scale, isoprene represents the dominant BVOC (440–600 Tg C yr^{-1}) with high emission factors from broadleaf trees including species of oak, willow, palm oil and eucalypt (Benjamin et al., 1996). Plants may release isoprene as part of a plant protection mechanism, produced during photosynthesis (Loreto and Sharkey, 1990), although other hypotheses exist (e.g. Sharkey and Monson (2017)). Isoprene has a chemical lifetime of approximately 1 h via oxidation by the hydroxyl radical, resulting in chemical products that contribute to ozone chemistry and the formation of organic aerosol (Carlton et al., 2009). As urban sprawl encroaches on natural ecosystems, emissions of BVOCs influence the formation of urban surface ozone and organic aerosol that at elevated concentrations are detrimental to human health. Consequently, these emissions are incorporated into regional air quality models to help mitigate the impacts of air pollution. Emissions of isoprene vary in response to a range of drivers, including temperature, photosynthetically active radiation (PAR), leaf area index, soil moisture and vapour-pressure deficit. Isoprene emissions therefore peak during warm, sunnier months during the growing season, impacting air quality in major cities influenced by upwind BVOC emissions from vegetation (e.g. Utembe et al. (2018)). Here we focus on south-eastern Australia, characterized by semi-arid climate, where soil moisture deficit is an important factor of stress for isoprene emissions, and use a range of model and observed soil moisture products to improve the simulated effect of this deficit on isoprene emission.

Drought has played a key role in shaping the Australian landscape, but large parts of Australia are suffering from a continuing, multi-decade decline in rainfall that has placed additional water stress on ecosystems (Keywood et al., 2017). The 2000–2010 decade was called the “millennium drought”, due to persistent and anomalous dry conditions (van Dijk et al., 2013) and ended with two very wet years associated with La Niña. Future climate projections for Australia show droughts occurring more frequently, lasting longer, and affecting larger geographical regions, particularly over south and east Australia (Irving et al., 2012). Projected changes in rainfall will undoubtedly impact isoprene emission rates in Australia.

Despite extensive and persistent drought conditions, south-eastern Australia hosts diverse ecosystems including those adapted to semi-arid climates. Adaptations include having large root-to-shoot ratios, deeper tap roots and narrow leaves (Brunner et al., 2015). These qualities can enable xeric species (those in arid environments) to continue transpiration for longer than other species without rain (Zhou et al., 2014). Geron et al. (2016) measured leaf level isoprene emissions from oak trees during severe drought conditions at a central US site and observed decreased emissions from most oak species but increased emissions from a drought tolerant oak species. Similarly, Llusia et al. (2016) measured leaf level emissions from two oak species with different drought tolerances at a semiarid Mediterranean site in Israel and observed a large difference in their response to summer drought. Experiments where droughts have been imposed show increased isoprene emissions, suggesting xeric species tend to be temperature sensitive rather than to water stress (Genard-Zielinski et al., 2018). Where heat stress and drought have been combined, Bamberger et al. (2017) found the degree of stomatal opening was not related to isoprene emission. These studies demonstrate that accurate simulations of drought response in biogenic emission models may require recognizing that drought stress differs among species. This could be accomplished with parameterizations that account for the relative fractions of drought tolerant and intolerant species within a landscape. However severe long-term drought that exceeds the normal conditions in an ecosystem, such as that experienced recently in Australia, may eventually cause isoprene emissions to decrease as available leaf carbon depletes due to reduced photosynthesis (Zheng et al., 2017).

We use the Model of Emissions of Gases and Aerosols from Nature (MEGAN) version 2.1 to provide a framework to describe isoprene emissions in Australian-based land biosphere models. MEGAN2.1 calculates BVOC emissions for 147 species in 19 compound classes (Guenther et al., 2012) by integrating information from a range of field and laboratory studies. In recent work, MEGAN2.1 was coupled to the CSIRO Chemical Transport Model (C-CTM) (Cope et al., 2009) to predict BVOCs across south-east Australia at spatial resolutions up to 3 km (Emmerson et al., 2016). These authors found that MEGAN2.1 overestimated the importance of isoprene by up to a factor of six, this highest value occurring after a storm caused an unusual vegetation stress response. Taking into account errors in basal emissions (Misztal et al., 2016), i.e. dividing emissions by a factor of three, did not suit all observed campaign data. Emmerson et al. (2016) postulated that isoprene emissions from two-year old sapling eucalypt trees are probably higher than emissions from adult trees, and that using these sapling data in the construction of the emission factor maps may have caused the isoprene overestimation. Other work has emphasized that using measurements from healthy and well-tended young trees in laboratories/greenhouses will not necessarily be representative of natural, wildtype vegetation (He et al. (2000)). Isoprene emission rates for adult, wildtype eucalypts across Australia are not known with certainty.

MEGAN2.1 describes the impact of drought on isoprene emission using a soil moisture activity factor that defines how close local soil moisture is to the wilting point of the underlying soil type (Guenther et al., 2012). As this particular parameterisation is uncertain (Potosnak et al., 2014) and the importance has not been widely demonstrated, the activity factor is generally set to one, so that isoprene emission is insensitive to soil moisture changes. Studies that do use this activity factor are typically hampered by a lack of measurements and a lack of detail in mapped soil products, e.g. soil type, soil moisture and wilting points (Muller et al., 2008). Huang et al. (2015) tested two different soil moisture products across Texas during drought years, and found that isoprene emissions were reduced by 12–70%, illustrating the level of uncertainty.

Despite the uncertainty, the literature shows models achieving the magnitudes of isoprene emission reductions required in Australia via inclusion of a soil moisture parameterisation. Muller et al. (2008) achieved a global 20% reduction in isoprene emissions leading to small differences between their model and measurements over Australia. Other results for Australia show isoprene reductions of 50% (Sindelarova et al., 2014), and 30%–60% reductions for northern Australia (Lathiere et al. (2010) and Henrot et al. (2017), respectively). Henrot et al. (2017) output soil activity factors showing a range of 0.5–0.8 in the south-east coastal region of Australia between 2000 and 2012, incorporating the millennium drought years. Jiang et al. (2018) detail the new MEGAN3 soil moisture algorithm, which extends beyond a simple soil wilting point threshold by including the impacts of drought on photosynthetic processes. Initial comparisons with MEGAN2.1 at an oak-hickory forest in Missouri were extremely promising, and when implemented in the global CLM4.5 model, reduced summertime isoprene emissions up to 15% in northern Australia.

It is now possible to obtain data on soil moisture from space, which

provides us with a spatially and temporally varying soil moisture parameter. By assimilating these data into existing soil moisture models, we reduce the errors in modelling observed variations of isoprene emissions. Through application of a soil moisture activity factor, we aim to better understand the size of other errors such as basal emissions. In the next section, we describe the observations used and the processes added to the C-CTM to calculate the soil moisture activity factors for MEGAN2.1. In section 3, we describe results from using two soil moisture models and explore the assimilation of new satellite observations on soil moisture activity factors in the C-CTM, assessing their impact on isoprene emissions for the first time. We conclude the paper in section 4.

2. Data and methods

2.1. Data

2.1.1. Field campaigns

Our work centres on the timing of five well-studied field campaigns all occurring near Sydney, south-east Australia; MUMBA – Measurements of Urban, Marine and Biogenic Air, SPS – Sydney Particle Studies 1 and 2, and campaigns at Bringelly and Randwick. This paper focuses on modelling isoprene emissions rather than atmospheric mixing ratios, but Proton Transfer Reaction Mass Spectrometry observations are available at each of the sites, see references in Table 1. The locations are shown in Fig. 1, together with the extent of the 3 km model grid domains discussed later.

2.1.2. Ground-based soil moisture measurements

The Australian national Cosmic Ray Soil Moisture Monitoring Facility (CosmOz) network (Hawdon et al. (2014)) has ten sites in Australia. The closest to Sydney is at Baldry (148.54°E, 32.87°S) operating between 30 March 2011 and 12 March 2014, overlapping with the SPS2 and MUMBA measurements. CosmOz measurements are based on counting neutrons produced from the interaction of cosmic rays with water molecules in the soil. A higher neutron count represents a lower soil moisture. Baldry is located in an area of wide pasture and has red podsolic soil, which is in a region classed as coarse/medium sandy loam. The depths of the CosmOz measurement varies; average depths across the SPS2 period are 25.7 cm (range 18.5–33.4 cm) and MUMBA are 33.1 cm (range 19.6–47.9 cm).

The Eucalyptus Free Air CO_2 Enrichment (EucFACE) facility at Hawkesbury (150.74°E, 33.62°S, Fig. 1) have made soil moisture measurements since late April 2012 (Gimeno et al., 2018). The experiment consists of six rings of towers surrounding the canopy, three in ambient air and three at CO_2 at 550 ppm. The surface soil is composed of 75% sand, with 30% clay below 50 cm. The soil moisture dataset includes daily observations made at 25 cm depth, and less frequent measurements taken at regular depth intervals down to 4.5 m. The Hawkesbury measurements overlap with our MUMBA field campaign.

2.1.3. Satellite observations of soil moisture

We use the daily aggregate data product from the Soil Moisture and Ocean Salinity (SMOS) satellite mission described on a 50 km spatial grid, with an accuracy of 0.04 $m^3 m^{-3}$ (Kerr et al., 2010). SMOS was launched into a 98.44° inclined orbit by the European Space Agency in November 2009. SMOS uses L-band passive microwave remote sensing to estimate the amount of water in the top 5 cm of soil, which closely corresponds to inputs from precipitation. Semi-arid rooting depths can access deeper water. Although changes in soil moisture observed by SMOS may not generally describe the limits of ecosystem access to groundwater, under extreme drought conditions when groundwater is significantly depleted it may be a reasonable approximation.

We use the Centre National D'Etudes Spatiales (CNES) L3 daily data product mapped at 25 km (Al Bitar et al., 2017) covering the SPS2 and MUMBA campaign periods. Dates where no SMOS data are available are 20th and 25th April 2012, 8th and 13th May 2012, 7th, 12th, 25th and 30th January 2013 and 12th February 2013.

2.2. The CSIRO Chemical Transport Model C-CTM

The C-CTM is a modelling framework consisting of modules representing meteorological, emissions, transport and deposition processes to both gas and aerosol phase species. The C-CTM has been used for air quality applications involving particles from smoke (Lawson et al., 2017), and shipping emissions (Broome et al., 2016) in addition to the biogenic modelling (Emmerson et al., 2016, 2018; Paton-Walsh et al., 2018).

The C-CTM comprises a four-way nested grid from 80 km to 3 km horizontal resolution, driven with meteorological data from the Conformal Cubic Atmospheric Model (CCAM, McGregor and Dix (2008)). The setup is similar to that described in Emmerson et al. (2016), but using the more recent 2008 anthropogenic emission inventory for the Sydney GMR (DECCW, 2012). Carbon Bond 5 (CB05) chemistry is used (Sarwar et al., 2008) and includes an updated toluene scheme (Sarwar et al., 2011). We focus this work on the isoprene emissions from MEGAN2.1 rather than volume mixing ratios at the measurement sites, thus will not concentrate on technicalities of the C-CTM.

Due to the high resolution of the inner C-CTM domain, Emmerson

Table 1
Details of measurement campaigns. PTR-MS = Proton Transfer Reaction Mass Spectrometry.

Campaign name	PTR-MS availability	Longitude and Latitude	Distance from Sydney	Land use	Data reference
MUMBA, Wollongong	22.12.12–15.02.13	150.8995 °E 34.3972 °S	65 km	Coastal, grass site with eucalypt escarpment 3 km to west	Paton-Walsh et al. (2017), Guérette et al. (2017)
SPS1, Westmead	18.02.11–07.03.11	150.9961°E 33.8014 °S	21 km	Suburban, grass site within hospital grounds	Keywood et al. (2016a)
Bringelly	24.01.07–27.02.07	150.7619 °E 33.9177 °S	45 km	Semi-rural, 16 km from dense eucalypt forest	Emmerson et al. (2018)
Randwick	28.02.07–19.03.07	151.2428 °E 33.9318 °S	8 km	Urban, within army barracks	Emmerson et al. (2018)
SPS2, Westmead	14.04.12–14.05.12	150.9961 °E 33.8014 °S	21 km	Suburban, grass site within hospital grounds	Keywood et al. (2016b)

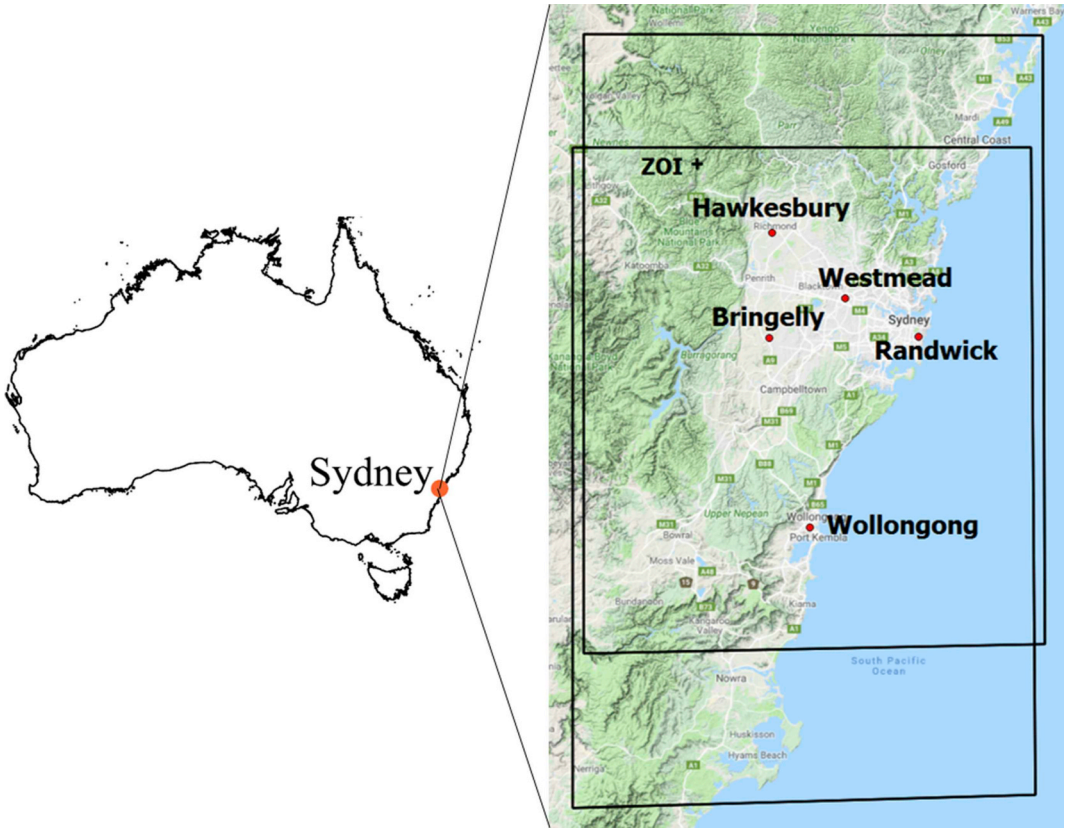

Fig. 1. Map to show locations of observations within Sydney (red spots), and extent of 3 km model domains. ZOI = zone of influence. Map produced by QGIS using Google Physical layer. (For interpretation of the references to colour in this figure legend, the reader is referred to the Web version of this article.)

et al. (2016) remapped a 1 km IGBP product from Belward et al. (1999) to the plant functional types (PFTs) required by MEGAN2.1. A MODIS MCD15A2 version 4 dataset is used for monthly LAI.

The approach for running MEGAN2.1 within the C-CTM uses a 1 km resolution isoprene emission factor map available from https://bai.ess.uci.edu/megan/versions/megan21. Whilst the isoprene emissions are not sensitive to the class of PFTs, they are sensitive to the grid cell fraction covered by the PFT, and thus the PFT distribution.

The inner 3 km domains are centred on either Westmead or Wollongong and extend for 180 km north-south and east-west (Fig. 1). The map shows the urban region of Sydney surrounded by eucalypt forests, particularly in the north and west, which are the source locations for the observed isoprene (Emmerson et al., 2018). Thus, the area to the north west in the 3 km domains becomes our 'zone of influence' (ZOI), marked with a + sign in Fig. 1, and soil moisture will be investigated here. The ZOI location is 150.40°E, 33.50°S and is positioned to sit within both inner model domains. We note that all the field campaigns conducted thus far in Sydney are contained within the urban region, and not in the forested ZOI.

2.3. Including the soil moisture activity factor in the C-CTM

The soil moisture activity factor, γSM, is a fraction between 0 and 1 that is applied directly to the isoprene emission calculations. It takes the following form in MEGAN2.1 (Guenther et al., 2012).

$$\gamma SM = 1 \qquad \theta > \theta_1 \tag{1a}$$

$$\gamma SM = \frac{\theta - \theta_{wt}}{c} \qquad \theta w_t < \theta < \theta_1 \tag{1b}$$

$$\gamma SM = 0 \qquad \theta < \theta w_t \tag{1c}$$

where θ is the volumetric soil moisture ($m^3\ m^{-3}$), θw is the wilting point ($m^3\ m^{-3}$) for soil type *t*, *c* is a constant (= 0.04), and θ_1 equals ($\theta w_t + c$). When a plant has ample access to water, γSM is returned as 1; similarly, when the plant has no access to water, γSM is 0. There is an intermediate situation when the soil moisture is close to the wilting point, controlled by *c*, causing the plant to emit decreasing levels of isoprene. We have adapted our model code similar to Huang et al. (2015) to output the value of γSM.

The constant *c*, not only affects the value of the denominator in the equation, but also limits the range above the wilting point that this equation is applied. Thus the value of *c* is subject to debate. In Guenther et al. (2006) $c = 0.06$, based on a single experiment on 2-year old oak trees in one soil type (commercial potting soil) from Pegoraro et al. (2007). The constant was decreased to 0.04 in Guenther et al. (2012) because emissions were being shut off in regions where there was no extreme drought.

We calculate γSM by incorporating the soil moisture from two models developed by CSIRO: a scheme developed for the Mk3.6 Global Climate Model (Gordon et al., 2002) (hereafter known as "MK"), and the newer Soil-Litter-Iso model (SLI) model for coupled heat, water and stable-isotope transport in soil (Haverd and Cuntz, 2010). Both soil models are related to the Community Atmosphere Biosphere Land Exchange model (CABLE) (Kowalczyk et al., 2013), and use a similar approach to transport water through the soil layers. SLI contains improvements over MK via enabling water to exist in the vapour phase and limiting evaporation at the soil/air interface by incorporating a litter layer. Allowing for a vapour phase is more appropriate for modelling soil moisture in arid regions. MK is the original scheme within CCAM and was the basis of the first soil scheme implemented within CABLE. The SLI model has since been incorporated into CABLE (Cuntz and Haverd, 2018; Haverd et al., 2016). A third CABLE configuration that includes the CABLE vegetation canopy parameterisation used by SLI, as well as a soil model similar to MK, is referred to as CABLE v2.2.3.

The soil moisture in CABLEv2.2.3 is more similar to SLI than MK, thus the reason for choosing MK provides diversity to achieve a range in results.

Both MK and SLI use similar soil texture descriptions. Each soil type, t has a predicted plant wilting point indicating the amount of water necessary for plant survival at each location (Table 2). Soil moisture is calculated for six layers (depths of 0.02m, 0.08m, 0.21m, 0.56m, 1.49m and 3.96m), with the surface layer containing 5% of the plant root system, and deeper layers containing 20%, 20%, 20%, 20% and 15% respectively. The value of θ becomes the root density weighted average (RDWA) volumetric soil moisture across all six soil layers. The mapped soil types in Sydney (Fig. 2) show a mainly sandy soil (type 1) with regions of coarse sandy loam in the urban region (type 4) and a small area of sandy clay to the west (type 7). The ZOI, marked with the + sign, is of soil type 1 (sand). Typically, sandy soil is well drained and does not hold much water, leading to lower wilting points than for other soil types. The soil types within Fig. 2 do not change with depth.

2.4. SMOS assimilation

We combine SMOS satellite soil moisture data, O, with the hourly modelled MK and SLI soil moisture data, M, to provide an assimilated soil moisture product, A_{SM}, at each time step to drive MEGAN:

$$A_{SM} = \frac{\sigma_M^2}{\sigma_O^2 + \sigma_M^2} O + \frac{\sigma_O^2}{\sigma_O^2 + \sigma_M^2} M \quad (2)$$

where σ_M^2 and σ_O^2 denote the errors the model and observations, respectively. We assume a model error of 100%. Analysis of SMOS data suggest a low measurement error of ~4% (Pierdicca et al. (2017). However we also adopt measurement errors of 15% and 50% to explore the sensitivity of measurements on the resulting isoprene emissions.

We smoothed the SMOS data in the horizontal dimension using Climate Data Operators (Schulzweida, 2018), limiting the hard edges in A_{SM} where no SMOS data are available, e.g. near the coasts. To limit further hard edges in A_{SM}, we only assimilate SMOS data if O is greater than half the wilting point for coarse sandy soil ($> 0.036\ m^3\ m^{-3}$); model soil moisture is used otherwise. We also consider how SMOS influences the vertical soil depth, as restricting the assimilation to the surface layer would influence just 5% of the RDWA. First, we limit the influence to the top three soil layers which represents 45% of the RDWA. Secondly, we allow SMOS to influence all six soil layers.

2.5. Sensitivity runs

The C-CTM is run with configurations shown in Table 3, across the five time periods of the field campaigns. The control run uses γSM = 1, whilst in other tests γSM is allowed to vary according to equations (1)–(3). A further test using γSM = 0.33 represents reducing the isoprene emission factors by a factor of three, as recommended in Emmerson et al. (2016). The SMOS assimilations take place from 2012 onwards coinciding with the SPS2 and MUMBA campaign periods.

3. Results and discussion

3.1. Model evaluation of soil moisture

Modelled soil moisture from Baldry is extracted from the 9 km domains as the CosmOz Baldry site is located outside of our inner 3 km domains. SLI has previously been evaluated for the 2012–2013 period with data from other CosmOz sites in Australia with good correlations > 0.77 (Holgate et al., 2016). The top two plots in Fig. 3 compares the CosmOz observations to the time series in surface level moisture measured by SMOS at Baldry as 24-h averages. CosmOz data is generally greater than SMOS by ~$0.04\ m^3\ m^{-3}$ during SPS2, but of similar magnitude during the early dry period of MUMBA. The peaks in SMOS later in the MUMBA period agree when the timings of the peaks occur in CosmOz, but are 0.1–$0.2\ m^3\ m^{-3}$ higher. These differences are attributed to the deeper levels the CosmOz measurements are taken (approx. 30 cm). The RDWA from soil levels 1–3 in MK and SLI soil moisture are plotted to correspond with these CosmOz data. SLI tends to predict higher soil moisture values than MK. The timings of the MK and SLI peaks correspond with the peaks in SMOS, but differ in magnitude. Nudging MK and SLI towards SMOS will reduce the value of θ for SPS2 and the first 15 days of MUMBA. However SLI soil moisture is already above the wilting point for soil types 1 and 4, so will not be impacted as much as MK. We considered whether to adjust SMOS values using the deeper CosmOz measurements, but there was no clear pattern of their differences.

The Hawkesbury moisture depth profiles are averaged onto similar levels to the models. The 8th January 2013 observed profile shows a very dry surface layer < $0.05\ m^3\ m^{-3}$, increasing to $0.14\ m^3\ m^{-3}$ at 0.5 m then increasing to $0.24\ m^3\ m^{-3}$ at 4 m. The second observed profile on 14th February 2013 also tends towards $0.24\ m^3\ m^{-3}$ at 4 m but includes a wetter sub-surface reaching $0.25\ m^3\ m^{-3}$ at 0.5 m. The models all tend towards $0.17\ m^3\ m^{-3}$ at 4 m. SLI captures the additional moisture in the surface layer of 14th February 2013, whereas the surface moisture in MK is less responsive and remains too dry. The observed profiles suggest the models are too dry at 4 m. If we calculate the RDWA for models and observations the results are more similar. On 8th January 2013 the RDWA is $0.11\ m^3\ m^{-3}$ in the observations and $0.15\ m^3\ m^{-3}$ for both MK and SLI. On 14th February 2013 the RDWA is $0.23\ m^3\ m^{-3}$ for the observations, $0.18\ m^3\ m^{-3}$ for MK and $0.23\ m^3\ m^{-3}$ for SLI. The shape in the Hawkesbury time series (bottom right panel) is captured by MK and SLI but neither model is dry enough during the first 20 days.

Fig. 4 shows the spatial distribution in surface moisture data (to 2 cm depth) for the SPS2 and MUMBA time periods from SMOS, MK and SLI. Both models show soil moisture less than $0.30\ m^3\ m^{-3}$, with the difference between MK and SLI being greater for SPS2 than MUMBA. The spatial distribution of the modelled soil moisture is entirely dependent on the distribution and limitations of the soil textures shown in Fig. 1. SLI uses a more spatially resolved land use map than MK, showing zero isoprene emitting waterbodies such as lakes in Fig. 4. The average surface layer soil moisture of MK and SLI are wetter than SMOS suggests. The range in SMOS soil moisture values in these domains is 0.04–$0.27\ m^3\ m^{-3}$, whereas the MK range is 0.06–$0.22\ m^3\ m^{-3}$ and for SLI is 0.06–$0.30\ m^3\ m^{-3}$.

The average soil moisture at the ZOI during SPS2 indicate levels of $0.12\ m^3\ m^{-3}$ from SMOS, $0.09\ m^3\ m^{-3}$ from MK (21% decrease) and $0.17\ m^3\ m^{-3}$ from SLI (42% increase). During the MUMBA period the ZOI soil moisture is $0.11\ m^3\ m^{-3}$ from SMOS, $0.10\ m^3\ m^{-3}$ for MK and $0.12\ m^3\ m^{-3}$ for SLI (11% decrease and 13% increase respectively). The wilting point for sandy soil is $0.07\ m^3\ m^{-3}$. If only the surface layer is taken into account, SMOS indicates the isoprene emission will not be impacted for SPS2 but begin to be impacted in MUMBA. MK is more likely than SLI to produce θ values in the range where γSM will be less

Table 2
Wilting points used for soil types shown in Fig. 2, derived from Post and Zobler (2000).

t	Description	Wilting point, θw $m^3\ m^{-3}$
1	Coarse sand/Loamy sand	0.072
2	Medium clay loam/silty clay loam/silt loam	0.216
3	Fine clay	0.286
4	Coarse-medium sandy loam/loam	0.135
5	Coarse-fine sandy clay	0.219
6	Medium-fine silty clay	0.283
7	Coarse-medium-fine sandy clay loam	0.175
8	Organic peat	0.395
9	Permanent ice	0.216

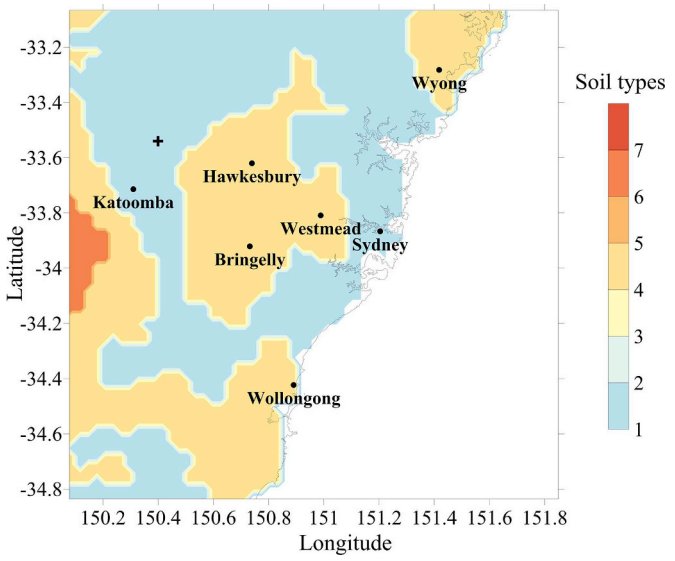

Fig. 2. Map of soil types in Sydney region. The colour scale refers soil types listed in Table 2. (For interpretation of the references to colour in this figure legend, the reader is referred to the Web version of this article.)

Table 3
Configurations of soil moisture sensitivity runs within C-CTM.

Model run	Soil activity factor, γSM
γSM = 1	1
MK_{no_SMOS}	Varied
SLI_{no_SMOS}	Varied
γSM = 0.33	0.33
A_{SM}MK 3L 15% (x4)	Varied using SMOS assimilation
A_{SM}SLI 3L 15% (x4)	Varied using SMOS assimilation

*The first number denotes either three or six soil layers which SMOS will influence; the second is the chosen observational error, either 15% or 50%.

than 1. However our calculation of γSM takes into account the RDWA soil moisture down to 4 m, which the surface SMOS data cannot provide a constraint on.

3.2. Changes in γSM

Domain average γSM is output spatially for MK_{NO_SMOS} and SLI_{NO_SMOS} models during each of the campaigns (Fig. 5, left and middle panels), ordered from January (MUMBA) through to May (SPS2). The patterns in the spatial plots correspond to rainfall patterns with drier regions shown in green/blue. The spatial distributions show SLI_{NO_SMOS} reaching a domain average γSM of 1 from SPS1 onwards, suggesting that there is ample moisture available in each soil type to be above θ_1 and isoprene emissions are not impacted. The MK_{NO_SMOS} model still has regions of γSM < 1 by SPS2, but reaches 1 in the coastal regions during SPS2, corresponding to coastal rainfall in NSW between 17–20 April 2012 reaching 10–15 cm (Bureau of Meteorology, 2017). The right hand panels of Fig. 5 show the time series in γSM at the ZOI, and here include output from Jiang et al. (2018) comparing to their MEGAN2.1 and MEGAN3 soil moisture parameterisations at the ZOI. MEGAN2.1 compares the level of moisture in the soil with the wilting point of that soil type, evaluating whether there is water stress. MEGAN3.0 builds on this parameterisation by investigating how this water stress impedes photosynthesis using $B_t = \sum w_i r_i$, where B_t is the soil water stress function, w is the wilting factor based on Clapp and Hornberger (1978) and r the fraction of the root system in soil layer i. The activity factor due to drought, γ_d is a value between 0 and 1 and applied to the isoprene emission rate. It is calculated by comparing B_t to a threshold value of 0.6 (equation (3)). This value was chosen as the best fit between modelled and measured isoprene emissions at the MOFLUX site in Ozarks, Missouri, USA.

$$\gamma_d = 1 \qquad B_t > 0.6 \tag{3a}$$

$$\gamma_d = \frac{V_{Cmax}}{\alpha} \qquad B_t < 0.6.\ \alpha = 37 \tag{3b}$$

$$\gamma_d = 0 \qquad B_t < 0.6 \tag{3c}$$

where Vcmax is the rate of carboxylation by the photosynthetic enzyme Rubisco, and α is a factor derived from measurements at the MOFLUX site.

Each campaign's domain average precipitation is also shown in Fig. 5 to demonstrate how γSM responds to the input of moisture. Generally γSM in all models responds to rainfall perturbations, tending towards 1. MK_{NO_SMOS} is drier than SLI_{NO_SMOS} on average by 17–39%, less in the autumnal months, more in summer. In all the profiles, MK_{NO_SMOS} is quicker to return to soil moisture deficit conditions after rain than SLI_{NO_SMOS}, suggesting MK_{NO_SMOS} requires sustained rainfall to maintain higher γSM values. MEGAN2.1 has a very smooth γSM profile in all campaigns, with little variation. The MEGAN3 γSM profile is more varied and follows the pattern in the SLI_{NO_SMOS} profile more than any other model, albeit at different magnitudes.

There are two distinct periods in γSM during MUMBA – a dry early January, followed by rain on 29 January and 2 February, corresponding with the timing of heavy rain beginning on 27 January after ex tropical cyclone Oswald passed over New South Wales (NSW) (BoM, 2017). During the drier period, γSM in MK_{NO_SMOS} reduces to 0.3 and in SLI_{NO_SMOS} to 0.5. After the rain γSM returns to unity in both models.

The domain average γSM is higher during SPS2 than for any other field campaign period. The peaks coincide with model rainfall up to 30 mm h^{-1} on 19th April, during the coastal rainfall observed in NSW (BoM, 2017). γSM declines after 1st May 2012 in MK_{NO_SMOS}, but not in SLI_{NO_SMOS} or Jiang et al.'s (2018) models. Observations of isoprene mixing ratios during SPS2 were over-predicted by a factor of ~2 (Emmerson et al., 2016), but the results here suggest that a soil moisture deficit will not improve the model predictions.

The other three field campaigns were very dry and incurred little rainfall. There are stronger impacts on γSM in MK_{NO_SMOS} and MEGAN3 than SLI_{NO_SMOS} and MEGAN2.1. γSM in MEGAN3 reduces to 0.1 during the Bringelly campaign, and shows a brief dry period during SPS1 at the beginning of March, that is only corroborated by the MK_{NO_SMOS} model. The results at Bringelly highlight that there is a large increase in γSM in all models when there has been a little rain (up to 4 mm h^{-1} on January 24th, 2007), suggesting soil moisture before the rain was maintained just under θ_1.

The SMOS assimilations nudge the modelled soil moisture towards the satellite measurements, and show an unsmooth profile. The SMOS time series profile back in Fig. 3 was predominantly lower than MK and SLI during SPS2, but showed periods of high and low soil moisture during MUMBA. This see-sawing is replicated in the γSM profile during both campaigns. The SLI soil moisture is higher than MK soil moisture during MUMBA, so is affected less by SMOS during this period. The 15% observational error choice is a stronger nudge towards the measurements than the 50% error; in Fig. 5 only the 3L 15% assimilation results are shown. Nudging soil moisture from three layers strongly towards the SMOS data (3L 15% tests) shows very different impacts on γSM for A_{SM}MK 3L 15% and A_{SM}SLI 3L 15%, suggesting that the choice of soil moisture model is critical. This result is also evident later in Fig. 7 in section 3.3, where we explore the impacts on isoprene emissions via the choice of observational error and number of soil layers assimilated.

3.2.1. Hourly or less frequent soil moisture input data?

Soil moisture in the surface soil layer responds rapidly to rainfall, with sublayers responding more slowly as water drains. This work uses the RDWA as input to equation $(1)_{(a,b,c)}$ which is less sensitive to surface

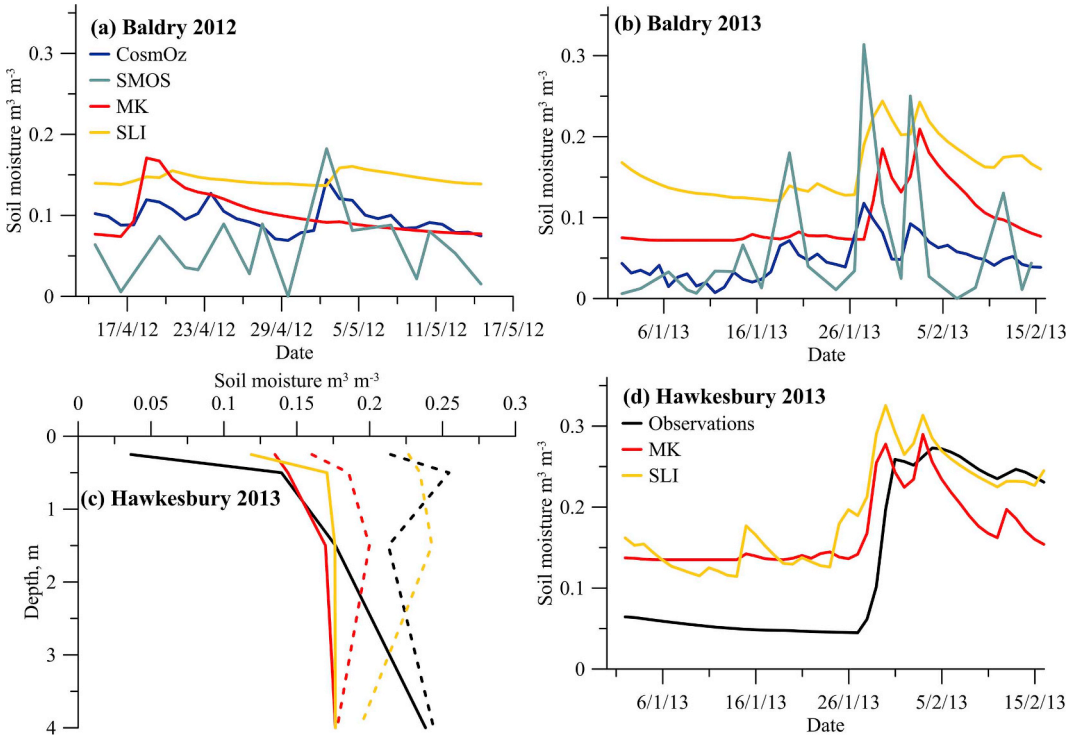

Fig. 3. Observed (CosmOz, Hawkesbury and SMOS) and model (MK and SLI) daily mean volumetric soil moisture ($m^3\ m^{-3}$). (a) and (b) are located at Baldry during SPS2 and MUMBA, whilst (c) and (d) are located at Hawkesbury during MUMBA only. Panels (a), (b) and (d) show time series. Panel (c) shows soil depth profiles for 8.1.13 (solid lines) and 14.2.13 (dashed lines).

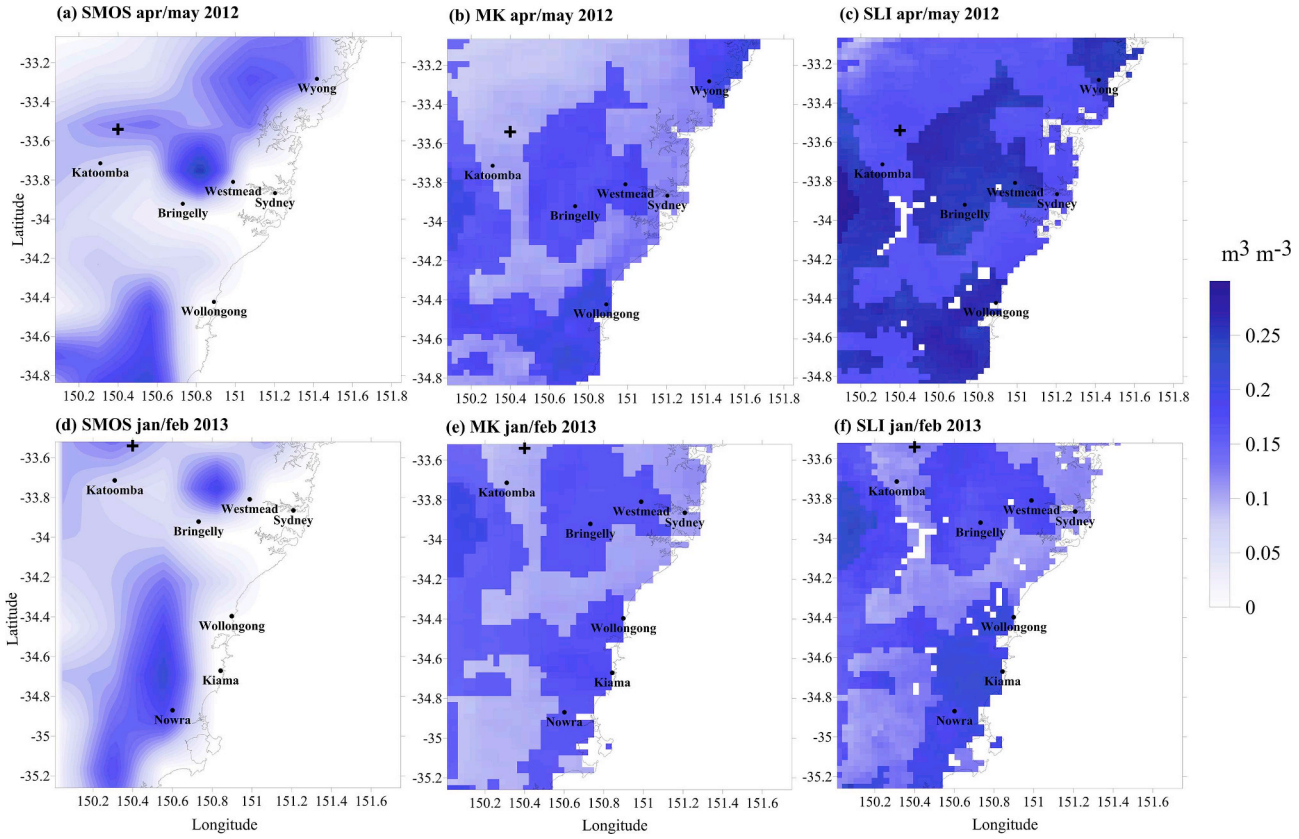

Fig. 4. Panels (a) and (d) Average surface soil moisture from the SMOS satellite product, (b) and (e) MK and (c) and (d) SLI across the Sydney region during the SPS2 (2012) and MUMBA (2013) campaigns. + sign marks the ZOI.

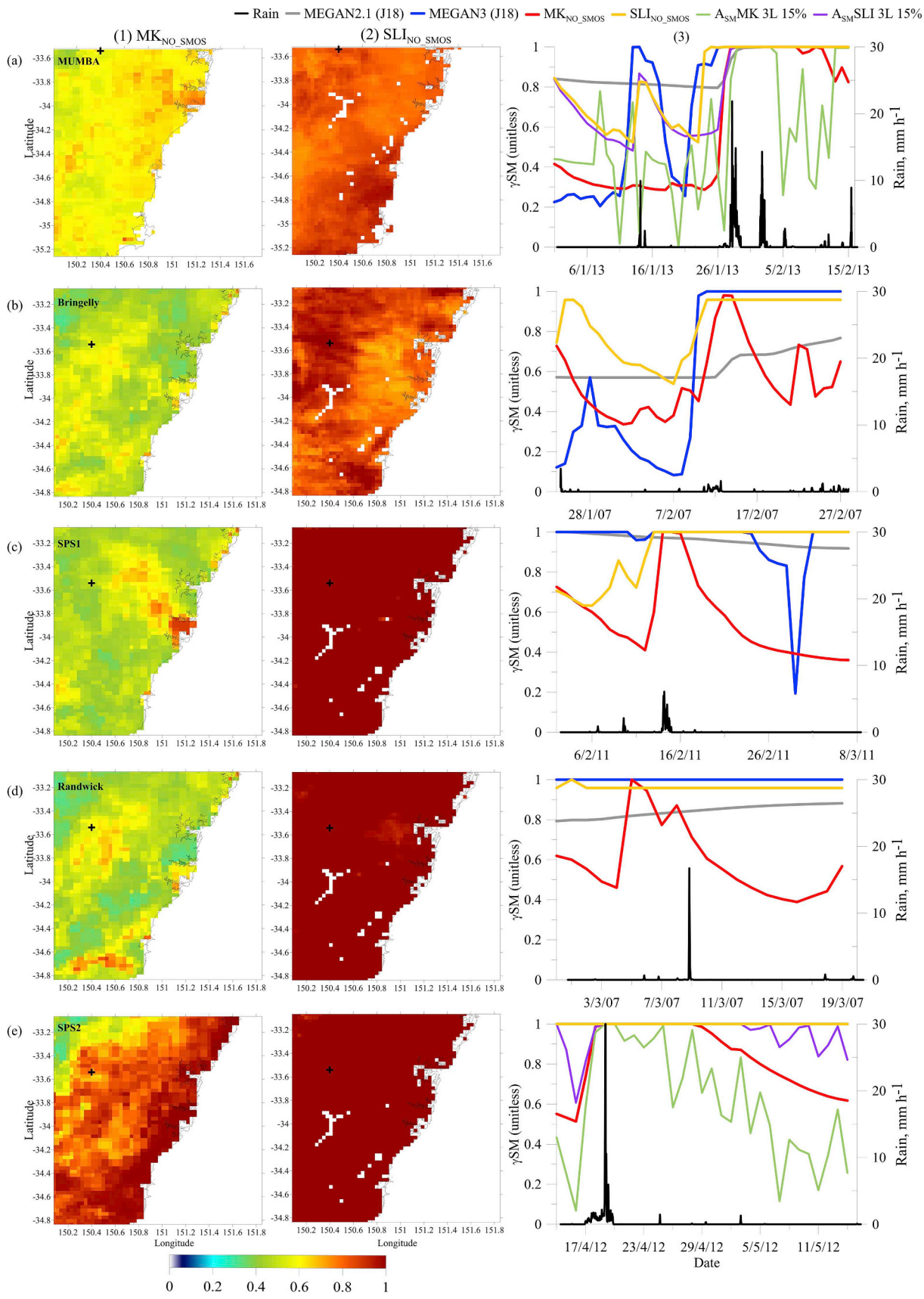

Fig. 5. Domain average γSM from MK_{NO_SMOS} (column 1) and SLI_{NO_SMOS} (column 2) during each field campaign, (a) MUMBA, (b) Bringelly, (c) SPS1, (d) Randwick and (e) SPS2. Column 3: time series in γSM at the Zone of Influence (+sign) comparing outputs from this work to modelled γSM from MEGAN2.1 and MEGAN3 in J18 = Jiang et al. (2018). Domain average rainfall plotted on second y-axes.

variations as the surface layer contains only 5% of the root system. The time series in soil moisture in the deepest model layer varies by less than 0.02 $m^3 m^{-3}$ in both MK and SLI across all field campaigns. To study the impact of temporal frequency of soil moisture input to the C-CTM, we plot the response of γSM resulting from SLI to hourly and 24-hourly soil moisture data at the ZOI (Fig. 6) during the MUMBA campaign. After minor rainfall occurs on 15th January the hourly response in γSM is quicker to return to drier conditions than the 24-hourly response in γSM, but the latter response does capture the timings of the peaks and troughs. The overall change in γSM between the two examples is 3%, meaning that the loss by only accessing daily data (e.g. satellite data) is small. The loss is perhaps even smaller because isoprene is not emitted at night, and some of the hourly γSM values are redundant. If a less frequent soil moisture input is used, for example to represent longer term drought impacts, the γSM profile would tend towards a fixed value. In the MUMBA example in Fig. 6, we see that inclusion of a 10 day rolling average soil moisture input leads to a 7% reduction in γSM overall, but that using an average monthly moisture input leads to a 5% increase in γSM in January. In February there is no change.

3.3. Spatial distribution in isoprene emissions

The impacts of including a soil moisture parameter on isoprene emissions are shown spatially for the timing of MUMBA, which incorporates the SMOS assimilation (Fig. 7). The isoprene emitted in the urban region of Sydney is less than 1 mg m^{-2} h^{-1} under most treatments, but reduces to < 0.2 mg m^{-2} h^{-1} in the γSM = 0.33 and SMOS assimilated A_{SM}MK soil moisture runs. Higher emissions are found at the ZOI, from 4.6 mg m^{-2} h^{-1} in the γSM = 1 run to 1.5 mg m^{-2} h^{-1} in the γSM = 0.33 run.

The sensitivity tests produce the biggest isoprene reductions in the eucalypt forested regions, shown in red in the γSM = 1 run. γSM = 0.33 shows the greatest overall isoprene reduction (67% on average), followed by MK_{NO_SMOS} (52% decrease) and the SMOS assimilated A_{SM}MK runs, then followed by SLI_{NO_SMOS} (24% decrease) and the suite of SLI runs.

The differences between the three and six layer SMOS assimilation runs are greater for A_{SM}SLI than A_{SM}MK at the ZOI. Isoprene emissions at the ZOI reduced from 2.01 mg m^{-2} h^{-1} in MK_{NO_SMOS} to 1.58 mg m^{-2} h^{-1} for A_{SM}MK 3L 15% and 1.56 mg m^{-2} h^{-1} for A_{SM}MK 6L 15%. The region to the SW is also influenced, but less so as localised rainfall causes an increase in SMOS. The isoprene at the ZOI in the SLI suite of runs reduces from 3.36 mg m^{-2} h^{-1} for SLI_{NO_SMOS} to 3.14 mg m^{-2} h^{-1} for A_{SM}SLI 3L 15% and 2.94 mg m^{-2} h^{-1} for A_{SM}SLI 6L 15%. Domain average isoprene emissions reduce by 58% for A_{SM}MK 6L 15%, and by 38% for A_{SM}SLI 6L 15% from the γSM = 1 run.

The spatial pattern in emissions from the SMOS assimilations are very similar between A_{SM}MK 3L and A_{SM}MK 6L (and accordingly for A_{SM}SLI), suggesting that the choice of how many soil layers to allow SMOS to influence is not as important as choice of soil moisture model. The Hawkesbury soil moisture depth profiles from Fig. 3 suggested both models were too dry at 4 m, thus constraining all six soil levels to surface SMOS data is probably too strong. There are also few differences (< 0.5 mg m^2 h^{-1}) in the nudging strength achieved using either 15% (strongest) to 50% (weaker) observational error. However higher emissions in the 3L 15% sensitivity test than 3L 50% in the region SW of Wollongong (shown in blue) are more evident in the A_{SM}MK assimilations than A_{SM}SLI.

3.4. Domain and campaign average isoprene emissions and mixing ratios

Fig. 8 shows relative frequency histograms of the domain average isoprene emissions (a-e), and average diurnal cycles of isoprene predictions and observations at each of the campaigns sites, showing the normalised mean bias (NMB) for each of the sensitivity runs (f-j). Transport and chemical processes away from the emission regions may mean that the model achieves a good comparison with the observations for the wrong reasons, but gives a basic idea about whether γSM is too strong.

In the relative frequency plots, the isoprene emissions are grouped into 1 mg m^{-2} h^{-1} bins for all campaigns except SPS2 which have 0.1 mg m^{-2} h^{-1} bins, reflecting the smaller range in values during this campaign. A Gaussian fit has been applied to these data. The peaks of the Gaussian distributions for the sensitivity studies are shifted to the left from the γSM = 1 run, from approximately 3 mg m^{-2} h^{-1} in the summer campaigns to less than 2 mg m^{-2} h^{-1}. The distribution for the SLI_{NO_SMOS} test has moved the peaks least, whilst the γSM = 0.33 test has moved the peaks the most, to around 1/3 of the γSM = 1 run levels (1 mg m^{-2} h^{-1} in summer campaigns and 0.2 mg m^{-2} h^{-1} for SPS2). The difference on the x-axis of the peaks is greater between MK_{NO_SMOS} and the A_{SM}MK SMOS assimilated runs rather than SLI_{NO_SMOS} and the A_{SM}SLI assimilated runs, as described in the previous section for MUMBA. However there is different pattern for SPS2 which show large reductions in where the peak sits for all SMOS assimilations apart from A_{SM}SLI 3L 15%. This particular run shows a 4% average reduction from the SLI_{NO_SMOS} test, whereas the A_{SM}MK 3L 15% test is a 10% reduction from the MK_{NO_SMOS} test. On average across summer months, the reduction in isoprene mixing ratios (from the γSM = 1 run) resulting from MK_{NO_SMOS} is 54%, and 24% using SLI_{NO_SMOS}. However A_{SM}MK 6L 15% achieves larger mixing ratio reductions of 70% and 49% for A_{SM}SLI 6L 15%, during MUMBA.

The relative amount by which the peaks in isoprene emissions have shifted to the left of the base run in the relative frequency plots are roughly linear with the reduction in the isoprene volume mixing ratios (right-hand panels of Fig. 8). In most cases the sensitivity tests reduce the γSM = 1 run isoprene mixing ratios significantly, by 50–70%. The simplest approach of fixing γSM to 0.33 was too strong an isoprene reduction in all campaigns, capping the emission reduction to 67% from section 3.3. The value of the NMB is reduced under all of the sensitivity tests compared to the γSM = 1 run. Where SMOS data is available, the NMB from the assimilated soil moisture tests reduces further than the tests using unassimilated soil moisture input data. Our sensitivity tests show that varying the error of the observed data had little impact on the NMB (< 0.02 MUMBA, < 0.07 SPS2, note: 50% observed error results not shown in Fig. 8, as too similar to 15% results), compared with the choice of number of soil layers (< 0.04 MUMBA, < 0.21 SPS2) with which to assimilate, and the choice of soil moisture model (< 1.19 MUMBA, < 0.42 SPS2). The greatest reduction in bias was found when assimilating six soil layers.

Thus there are improvements to be gained in the modelled bias by

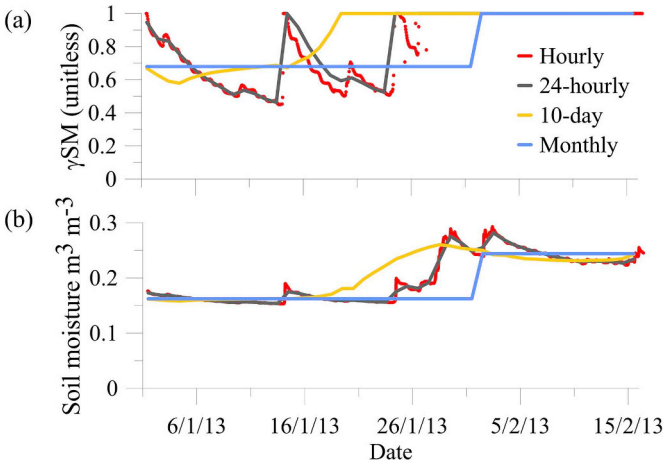

Fig. 6. (a) Difference in γSM achieved for (b) RDWA input frequency of different time periods. Data from the SLI model during the MUMBA campaign, at the ZOI.

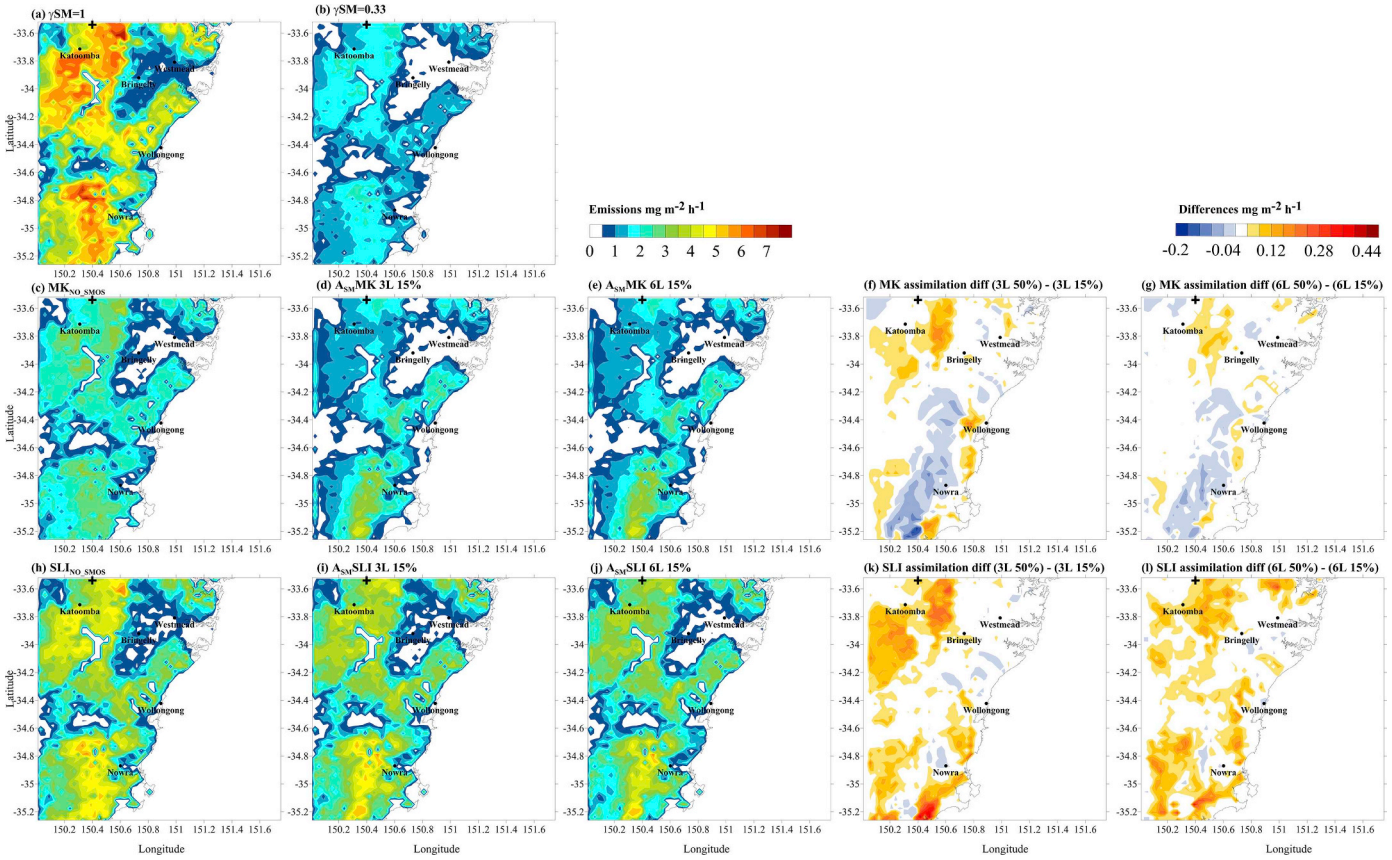

Fig. 7. Campaign average isoprene emissions for the different scenarios run across the MUMBA campaign period. (a) γSM = 1, (b) γSM = 0.33, panels (c–g) the MK suite of runs, panels (h–l) show the SLI suite of runs. Panels (f), (g), (k) and (l) show differences in emissions due to the nudging strength towards SMOS, at the specified soil levels.

inclusion of spatial and temporal variation in soil moisture variables. However there are still periods when the soil moisture parameterisation is not sufficient to reconcile the model with observations, suggesting that additional environmental processes may be missing from the C-CTM.

4. Conclusions

The aim of this paper was to (i) provide soil moisture values assessed by different soil moisture models (MK, SLI and a model constrained by SMOS satellite observations of soil moisture), and (ii) assess the sensitivity of isoprene according to these different soil moisture values, via a coupling between soil moisture models and MEGAN2.1. Plants decrease their emissions of isoprene when available water is limited during severe droughts. Severe droughts may also impact plant growth and limit biomass production, ultimately reducing the capacity for isoprene emission. It should be recognized that there are drought-tolerant and drought-intolerant plant species of the same plant functional type that occur within the same landscape and have very different drought responses. Accurate simulation of isoprene drought response may need to account for the relative fraction of drought tolerant plants in a landscape. Australia has experienced drought conditions for many years, predicted to increase in length and geographical extent in future. Whilst native vegetation is well adapted to drought, previous emission factor measurements have been conducted on healthy young trees in laboratories/glasshouses that are generally well watered and fertilised (He et al., 2000). These are not representative of semi-arid Australian conditions, and our isoprene emission adjustment using γSM goes someway to correct this. Any remaining modelled bias helps to gain a better understanding of the errors in the basal emission factors.

We calculated the impact of γSM on isoprene emissions over Australian eucalypt forests, using MK and SLI soil moisture driven models and a model that was constrained by SMOS satellite observations of soil moisture. To the authors' knowledge, our work represents the first application of satellite observations of soil moisture to quantifying isoprene emissions. We evaluated our model calculations using a small range of in situ soil moisture and isoprene PTR-MS mixing ratios in and around Sydney.

The SMOS data correlated well with Baldry CosmOz data with a shift of 0.04 $m^3\,m^{-3}$ in SPS2, and were similar during MUMBA, though the depths of the measurements were different. Surface MK and SLI soil moisture were of a similar magnitude range, and the timings of the peaks were good. Spatially the position of the higher SMOS soil moisture was in approximately similar locations to the models – themselves being dominated by the underlying soil type map.

The Hawkesbury observations included depth profiles on two days which showed SLI predicted soil moisture well at the surface, but both SLI and MK were too dry at 4 m. As the RDWA is used in this work, the comparison between SLI and the observations is reduced to 0.04 $m^3\,m^{-3}$ on the 8th January and 0 $m^3\,m^{-3}$ on 14th February. MK is drier than SLI on average by 17–39%, less in the autumnal months, more in summer. SLI is expected to predict soil moisture more accurately than MK due to inclusion of a moisture vapour phase and soil litter layer. Using SLI within MEGAN2.1 (SLI_{NO_SMOS}) yielded an average decrease of 24% in isoprene emissions during summer.

A number of sensitivity tests investigated how the SMOS data was assimilated with the MK and SLI soil moisture, by changing the SMOS data error and the number of model soil layers SMOS could influence. The application of any SMOS treatment has a greater impact on A_{SM}MK, reducing the domain average emissions by 58%, and A_{SM}SLI by 38%

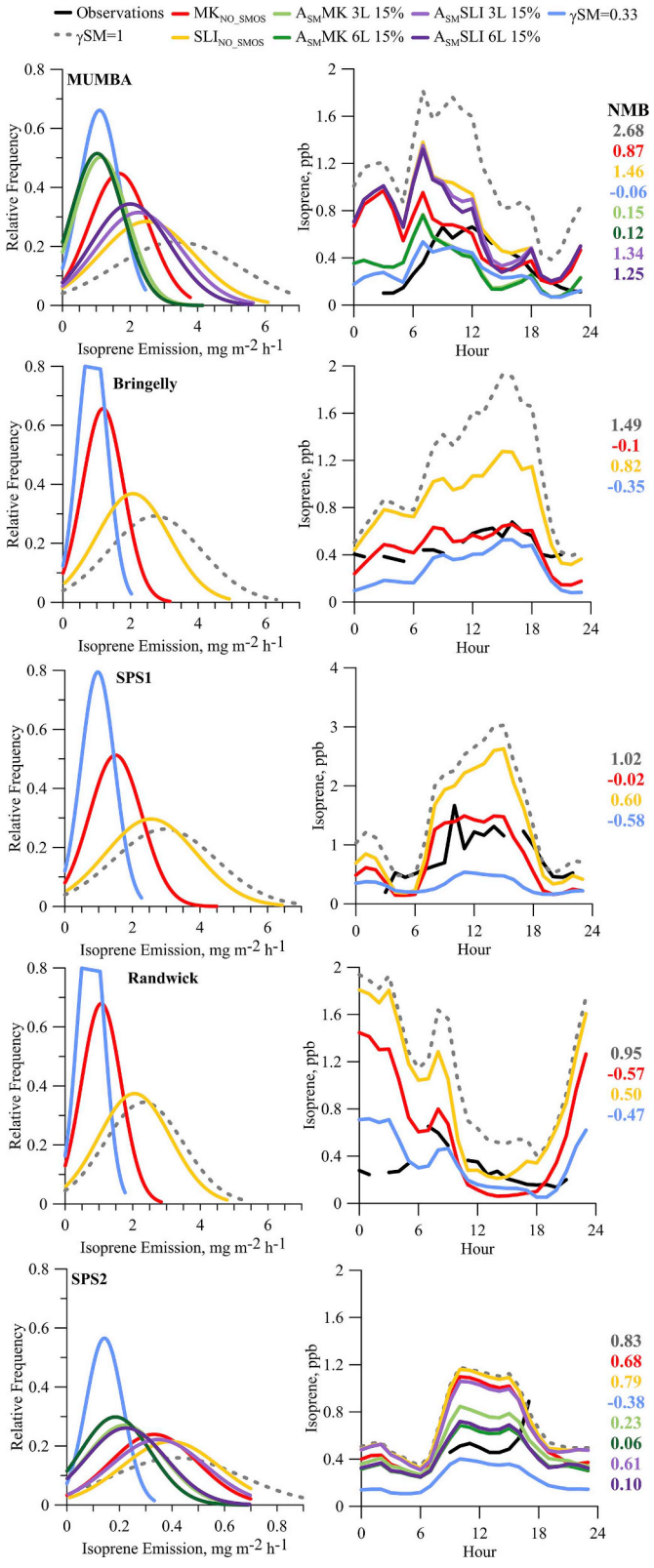

Fig. 8. (a–e) Relative frequency of domain average emission fluxes. (f–j) Campaign average diurnal cycles of volume mixing ratios for isoprene (right) at each of the field campaign sites: (a and f) MUMBA, (b and g) Bringelly, (c and h) SPS1, (d and i) Randwick and (e and j) SPS2. Values of the Normalised Mean Bias between model and observations given on right-hand side.

from the base γSM = 1 run during MUMBA. All sensitivity tests reduced the overall bias between modelled and observed isoprene mixing ratios. The spatial pattern in emissions from the SMOS assimilations are very similar between A_{SM}MK 3L and A_{SM}MK 6L (and accordingly for A_{SM}SLI), suggesting that the choice of how many soil layers to allow SMOS to influence is not as important as choice of soil moisture model. However assimilating all six soil layers using surface satellite data is probably too strong. There are also few differences ($< 0.5\ mg\ m^2\ h^{-1}$) in the nudging strength achieved using either 15% (strongest) to 50% (weaker) observational error. Different spatial patterns emerged for the SMOS assimilated runs according to rainfall positions and how close the modelled soil moisture was to the wilting point.

The simplest approach fixing γSM to 0.33 reduced isoprene predicted at the field sites too far, thus capping the required isoprene emission reduction to 67%. Increasing the complexity to using a time varying soil moisture parameter is a better choice, as it takes changing environmental conditions into account. As SLI is the more accurate soil moisture model, the errors in the basal emission factors are likely between 29% (SMOS assimilated) and 43% (unassimilated). The model uses RDWA soil moisture to calculate γSM, which smooths out the temporally frequent changes in the surface soil layer due to rainfall perturbations. We showed that the difference between using hourly or 24 hourly input data was only 3% across the MUMBA campaign, meaning quality is not lost if relying on daily satellite data as input. The real loss is even smaller, as there are no isoprene emissions at night. Use of a less frequent monthly soil moisture input led to a minor (5%) increase in γSM.

Despite the uncertainties, we recommend soil moisture is included when modelling isoprene in Australia, as biases can be reduced even if soil moisture is not fitted to satellite data. The spatial resolution of the SMOS observations were coarser than the model resolution (25 km versus 3 km), though we anticipate that these data will improve in future. The modelling approach we have taken and the results we report are relevant to studying semi-arid ecosystems across the world (e.g., Africa), where there are few in situ measurements available, but satellite coverage is good. However, our simple SMOS assimilation method can be used for constraining soil moisture models in observation-rich regions of the world to further improve predictive capability.

Our work is also relevant to Australian urban air quality, where geographically isolated cities are downwind of large expanses of vegetation. In summer, air masses laden with BVOCs mix with the urban airshed and result in perturbations of the photochemical environment. Predictions show drought conditions will be more prevalent in Australia, therefore air quality assessments need to account for how the biosphere will influence urban atmospheric chemistry in future.

Data provision

The LAI data product was retrieved from MCD15A2 version 4 from the online Data Pool, courtesy of the NASA Land Processes Distributed Active Archive Center (LP DAAC), USGS/Earth Resources Observation and Science (EROS) Center, Sioux Falls, South Dakota, https://lpdaac.usgs.gov/data_access/data_pool. PTR-MS datasets are available for MUMBA (https://doi.pangaea.de/10.1594/PANGAEA.871982), SPS1 (http://doi.org/10.4225/08/57903B83D6A5D) and SPS2 (http://doi.org/10.4225/08/5791B5528BD63). CosmOz data is available from http://www.ermt.csiro.au/html/cosmoz.html.

Acknowledgements

KME acknowledges funding from the Clean Air and Urban Landscapes Hub, which is a project of the Department of the

Environment's National Environmental Science Program. We acknowledge Belinda Medlyn at the Hawkesbury Institute for the Environment for advice on using their data, David McJannet for provision and processing of the CSIRO funded CosmOz network data, and Eva Kowalczyk and Cathy Trudinger at CSIRO for helpful discussions. ABG was supported by National Science Foundation (NSF) Atmospheric Chemistry program award AGS-1643042.

Appendix A. Supplementary data

Supplementary data to this article can be found online at https://doi.org/10.1016/j.atmosenv.2019.04.038.

References

Al Bitar, A., Mialon, A., Kerr, Y.H., Cabot, F., Richaume, P., Jacquette, E., Quesney, A., Mahmoodi, A., Tarot, S., Parrens, M., Al-Yaari, A., Pellarin, T., Rodriguez-Fernandez, N., Wigneron, J.P., 2017. The global SMOS Level 3 daily soil moisture and brightness temperature maps. Earth Syst. Sci. Data 9, 293–315. https://doi.org/10.5194/essd-9-293-2017.

Bamberger, I., Ruehr, N.K., Schmitt, M., Gast, A., Wohlfahrt, G., Arneth, A., 2017. Isoprene emission and photosynthesis during heatwaves and drought in black locust. Biogeosciences 14, 3649–3667. https://doi.org/10.5194/bg-14-3649-2017.

Belward, A.S., Estes, J.E., Kline, K.D., 1999. The IGBP-DIS global 1-km land-cover data set DISCover: a project overview. Photogramm. Eng. Rem. Sens. 65, 1013–1020.

Benjamin, M.T., Sudol, M., Bloch, L., Winer, A.M., 1996. Low-emitting urban forests: a taxonomic methodology for assigning isoprene and monoterpene emission rates. Atmos. Environ. 30, 1437–1452. https://doi.org/10.1016/1352-2310(95)00439-4.

Bureau of Meteorology, 2017. Climate summaries archive. 9.6.17. http://www.bom.gov.au/climate/current/statement_archives.shtml?region=nsw&period=month.

Broome, R.A., Cope, M.E., Goldsworthy, B., Goldsworthy, L., Emmerson, K., Jegasothy, E., Morgan, G.G., 2016. The mortality effect of ship-related fine particulate matter in the Sydney greater metropolitan region of NSW, Australia. Environ. Int. 87, 85–93. https://doi.org/10.1016/j.envint.2015.11.012.

Brunner, I., Herzog, C., Dawes, M.A., Arend, M., Sperisen, C., 2015. How tree roots respond to drought. Front. Plant Sci. 6, 00547 ARTN 547 10.3389/fpls.2015.

Carlton, A.G., Wiedinmyer, C., Kroll, J.H., 2009. A review of Secondary Organic Aerosol (SOA) formation from isoprene. Atmos. Chem. Phys. 9, 4987–5005. https://doi.org/10.5194/acp-9-4987-2009.

Clapp, R.B., Hornberger, G.M., 1978. Empirical equations for some soil hydraulic-properties. Water Resour. Res. 14, 601–604. https://doi.org/10.1029/WR014i004p00601.

Cope, M.E., Lee, S., Noonan, J., Lilley, B., Hess, D., Azzi, M., 2009. Chemical Transport Model: Technical Description. CSIRO Marine and Atmospheric Research Internal Report.

Cuntz, M., Haverd, V., 2018. Physically accurate soil freeze-thaw processes in a global land surface scheme. J. Adv. Model. Earth Syst. 10, 54–77. https://doi.org/10.1002/2017ms001100.

DECCW, 2012. Air Emissions Inventory for the Greater Metropolitan Region in New South Wales. Calendar Year 2008, Report. .

Emmerson, K.M., Galbally, I.E., Guenther, A.B., Paton-Walsh, C., Guerette, E.A., Cope, M.E., Keywood, M.D., Lawson, S.J., Molloy, S.B., Dunne, E., Thatcher, M., Karl, T., Maleknia, S.D., 2016. Current estimates of biogenic emissions from eucalypts uncertain for southeast Australia. Atmos. Chem. Phys. 16, 6997–7011. https://doi.org/10.5194/acp-16-6997-2016.

Emmerson, K.M., Cope, M.E., Galbally, I.E., Lee, S., Nelson, P.F., 2018. Isoprene and monoterpene emissions in south-east Australia: comparison of a multi-layer canopy model with MEGAN and with atmospheric observations. Atmos. Chem. Phys. 18, 7539–7556. https://doi.org/10.5194/acp-18-7539-2018.

Genard-Zielinski, A.C., Boissard, C., Ormeno, E., Lathiere, J., Reiter, I.M., Wortham, H., Orts, J.P., Temime-Roussel, B., Guenet, B., Bartsch, S., Gauquelin, T., Fernandez, C., 2018. Seasonal variations of Quercus pubescens isoprene emissions from an in natura forest under drought stress and sensitivity to future climate change in the Mediterranean area. Biogeosciences 15, 4711–4730. https://doi.org/10.5194/bg-15-4711-2018.

Geron, C., Daly, R., Harley, P., Rasmussen, R., Seco, R., Guenther, A., Karl, T., Gu, L.H., 2016. Large drought-induced variations in oak leaf volatile organic compound emissions during PINOT NOIR 2012. Chemosphere 146, 8–21. https://doi.org/10.1016/j.chemosphere.2015.11.086.

Gimeno, T., McVicar, T., O'Grady, A., Tissue, D., Ellsworth, D., 2018. EucFACE Hydrological andMeteorological Measurements from 2012-04-30 to 2014-11-15. Western Sydney University. http://doi.org/10.4225/35/5ab9bd1e2f4fb.

Gordon, H.B., Rotstayn, L.D., McGregor, J.L., Dix, M.R., Kowalczyk, E.A., O'Farell, S.P., Waterman, L.J., Hirst, A.C., Wilson, S.G., Collier, M.A., Watterson, I.G., Elliot, T.I., 2002. The CSIRO Mk3 Climate Sysyem Model. CSIRO, Australia. https://publications.csiro.au/rpr/download?pid=procite:ff94db7e-ad41-40bf-b6be-2ab1ad07805c&dsid=DS1.

Guenther, A., Karl, T., Harley, P., Wiedinmyer, C., Palmer, P.I., Geron, C., 2006. Estimates of global terrestrial isoprene emissions using MEGAN (model of emissions of gases and aerosols from nature). Atmos. Chem. Phys. 6, 3181–3210.

Guenther, A.B., Jiang, X., Heald, C.L., Sakulyanontvittaya, T., Duhl, T., Emmons, L.K., Wang, X., 2012. The Model of Emissions of Gases and Aerosols from Nature version 2.1 (MEGAN2.1): an extended and updated framework for modeling biogenic emissions. Geosci. Model Dev. (GMD) 5, 1471–1492. https://doi.org/10.5194/gmd-5-1471-2012.

Guérette, E.-A., Paton-Walsh, C., Kubistin, D., Humphries, R., Bhujel, M., Buchholz, R.R., Chambers, S., Cheng, M., Davy, P., Dominick, D., Galbally, I., Griffith, D.W.T., Griffiths, A., Keywood, M., Lawson, S., Molloy, S., Selleck, P., Simmons, J., Wilson, S.R., 2017. Measurements of Urban, Marine and Biogenic Air (MUMBA): Characterisation of Trace Gases and Aerosol at the Urban, Marine and Biogenic Interface in Summer in Wollongong, Australia. https://doi.org/10.1594/PANGAEA.871982.

Haverd, V., Cuntz, M., 2010. Soil-Litter-Iso: a one-dimensional model for coupled transport of heat, water and stable isotopes in soil with a litter layer and root extraction. J. Hydrol. 388, 438–455. https://doi.org/10.1016/j.jhydrol.2010.05.029.

Haverd, V., Cuntz, M., Nieradzik, L.P., Harman, I.N., 2016. Improved representations of coupled soil-canopy processes in the CABLE land surface model (Subversion revision 3432). Geosci. Model Dev. (GMD) 9, 3111–3122. https://doi.org/10.5194/gmd-9-3111-2016.

Hawdon, A., McJannet, D., Wallace, J., 2014. Calibration and correction procedures for cosmic-ray neutron soil moisture probes located across Australia. Water Resour. Res. 50, 5029–5043. https://doi.org/10.1002/2013wr015138.

He, C.R., Murray, F., Lyons, T., 2000. Monoterpene and isoprene emissions from 15 Eucalyptus species in Australia. Atmos. Environ. 34, 645–655. https://doi.org/10.1016/S1352-2310(99)00219-8.

Henrot, A.J., Stanelle, T., Schroder, S., Siegenthaler, C., Taraborrelli, D., Schultz, M.G., 2017. Implementation of the MEGAN (v2.1) biogenic emission model in the ECHAM6-HAMMOZ chemistry climate model. Geosci. Model Dev. (GMD) 10, 903–926. https://doi.org/10.5194/gmd-10-903-2017.

Holgate, C.M., De Jeu, R.A.M., van Dijk, A.I.J.M., Liu, Y.Y., Renzullo, L.J., Vinodkumar, Dharssi, I., Parinussa, R.M., Van der Schalie, R., Gevaert, A., Walker, J., McJannet, D., Cleverly, J., Haverd, V., Trudinger, C.M., Briggs, P.R., 2016. Comparison of remotely sensed and modelled soil moisture data sets across Australia. Remote Sens. Environ. 186, 479–500. https://doi.org/10.1016/j.rse.2016.09.015.

Huang, L., McGaughey, G., McDonald-Buller, E., Kimura, Y., Allen, D.T., 2015. Quantifying regional, seasonal and interannual contributions of environmental factors on isoprene and monoterpene emissions estimates over eastern Texas. Atmos. Environ. 106, 120–128. https://doi.org/10.1016/j.atmosenv.2015.01.072.

Irving, D.B., Whetton, P., Moise, A.F., 2012. Climate projections for Australia: a first glance at CMIP5. Aust Meteorol Ocean 62, 211–225.

Jiang, X.Y., Guenther, A., Potosnak, M., Geron, C., Seco, R., Karl, T., Kim, S., Gu, L.H., Pallardy, S., 2018. Isoprene emission response to drought and the impact on global atmospheric chemistry. Atmos. Environ. 183, 69–83. https://doi.org/10.1016/j.atmosenv.2018.01.026.

Kerr, Y.H., Waldteufel, P., Wigneron, J.P., Delwart, S., Cabot, F., Boutin, J., Escorihuela, M.J., Font, J., Reul, N., Gruhier, C., Juglea, S.E., Drinkwater, M.R., Hahne, A., Martin-Neira, M., Mecklenburg, S., 2010. The SMOS mission: new tool for monitoring key elements of the global water cycle. P Ieee 98, 666–687. https://doi.org/10.1109/Jproc.2010.2043032.

Keywood, M., Selleck, P., Galbally, I., Lawson, S., Powell, J., Cheng, M., Gillett, R., Ward, J., Harnwell, J., Dunne, E., Boast, K., Reisen, F., Molloy, S., Griffiths, A., Chambers, S., Crumeyrolle, S., Zhang, C., Zeng, J., Fedele, R., 2016a. Sydney particle study 1 - aerosol and gas data collection. v3. CSIRO. Data Collection. http://doi.org/10.4225/08/57903B83D6A5D_2016a.

Keywood, M., Selleck, P., Galbally, I., Lawson, S., Powell, J., Cheng, M., Gillett, R., Ward, J., Harnwell, J., Dunne, E., Boast, K., Reisen, F., Molloy, S., Griffiths, A., Chambers, S., Humphries, R., Guerette, E.-A., Cohen, D., 2016b. Sydney Particle Study 2 - Aerosol and Gas Data Collection. v1. CSIRO. Data Collection. http://doi.org/10.4225/08/5791B5528BD63_2016b.

Keywood, M., Hibberd, M., Emmerson, K., 2017. Australia State of the Environment 2016: Atmosphere, Independent Report to the Australian Government Minister for the Environment and Energy. Australian Government Department of the Environment and Energy, Canberra.

Kowalczyk, E.A., Stevens, L., Law, R.M., Dix, M., Wang, Y.P., Harman, I.N., Haynes, K., Srbinovsky, J., Pak, B., Ziehn, T., 2013. The land surface model component of ACCESS: description and impact on the simulated surface climatology. Aust Meteorol Ocean 63, 65–82.

Lathiere, J., Hewitt, C.N., Beerling, D.J., 2010. Sensitivity of isoprene emissions from the terrestrial biosphere to 20th century changes in atmospheric CO2 concentration, climate, and land use. Glob. Biogeochem. Cycles 24https://doi.org/10.1029/2009gb003548. Artn Gb1004.

Lawson, S.J., Cope, M., Lee, S., Galbally, I.E., Ristovski, Z., Keywood, M.D., 2017. Biomass burning at Cape Grim: exploring photochemistry using multi-scale modelling. Atmos. Chem. Phys. 17, 11707–11726. https://doi.org/10.5194/acp-17-11707-2017.

Llusia, J., Roahtyn, S., Yakir, D., Rotenberg, E., Seco, R., Guenther, A., Penuelas, J., 2016. Photosynthesis, stomatal conductance and terpene emission response to water availability in dry and mesic Mediterranean forests. Trees Struct. Funct. 30, 749–759. https://doi.org/10.1007/s00468-015-1317-x.

Loreto, F., Sharkey, T.D., 1990. A gas-exchange study of photosynthesis and isoprene emission in quercus-rubra L. Planta 182, 523–531. https://doi.org/10.1007/Bf02341027.

McGregor, J.L., Dix, M.R., 2008. An updated description of the Conformal-Cubic atmospheric model. In: Ohfuchi, K. H. a. W. (Ed.), High Resolution Numerical Modelling of the Atmosphere and Ocean. Springer, pp. 51–75.

Misztal, P.K., Avise, J.C., Karl, T., Scott, K., Jonsson, H.H., Guenther, A.B., Goldstein, A.H., 2016. Evaluation of regional isoprene emission factors and modeled fluxes in California. Atmos. Chem. Phys. 16, 9611–9628. https://doi.org/10.5194/acp-16-

9611-2016.
Muller, J.F., Stavrakou, T., Wallens, S., De Smedt, I., Van Roozendael, M., Potosnak, M.J., Rinne, J., Munger, B., Goldstein, A., Guenther, A.B., 2008. Global isoprene emissions estimated using MEGAN, ECMWF analyses and a detailed canopy environment model. Atmos. Chem. Phys. 8, 1329–1341.
Paton-Walsh, C., Guerette, E.A., Kubistin, D., Humphries, R., Wilson, S.R., Dominick, D., Galbally, I., Buchholz, R., Bhujel, M., Chambers, S., Cheng, M., Cope, M., Davy, P., Emmerson, K., Griffith, D.W.T., Griffiths, A., Keywood, M., Lawson, S., Molloy, S., Rea, G., Selleck, P., Shi, X., Simmons, J., Velazco, V., 2017. The MUMBA campaign: measurements of urban, marine and biogenic air. Earth Syst. Sci. Data 9, 349–362. https://doi.org/10.5194/essd-9-349-2017.
Paton-Walsh, C., Guérette, É.-A., Emmerson, K., Cope, M., Kubistin, D., Humphries, R., Wilson, S., Buchholz, R., Jones, N., Griffith, D., Dominick, D., Galbally, I., Keywood, M., Lawson, S., Harnwell, J., Ward, J., Griffiths, A., Chambers, S., 2018. Urban air quality in a coastal city: Wollongong during the MUMBA campaign. Atmosphere 9, 500. https://doi.org/10.3390/atmos9120500.
Pegoraro, E., Potosnak, M.J., Monson, R.K., Rey, A., Barron-Gafford, G., Osmond, C.B., 2007. The effect of elevated CO2, soil and atmospheric water deficit and seasonal phenology on leaf and ecosystem isoprene emission. Funct. Plant Biol. 34, 774–784. https://doi.org/10.1071/Fp07021.
Pierdicca, N., Fascetti, F., Pulvirenti, L., Crapolicchio, R., 2017. Error characterization of soil moisture satellite products: retrieving error cross-correlation through extended quadruple collocation. Ieee J-Stars 10, 4522–4530. https://doi.org/10.1109/Jstars.2017.2714025.
Post, W.M., Zobler, L., 2000. Global Soil Types, 0.5-Degree Grid (Modified Zobler). Oak Ridge National Laboratory Distributed Active Archive Center, Oak Ridge, Tennessee, U.S.A. https://doi.org/10.3334/ORNLDAAC/540. Data set. Available on-line. http://www.daac.ornl.gov.
Potosnak, M.J., LeStourgeon, L., Pallardy, S.G., Hosman, K.P., Gu, L.H., Karl, T., Geron, C., Guenther, A.B., 2014. Observed and modeled ecosystem isoprene fluxes from an oakdominated temperate forest and the influence of drought stress. Atmos. Environ. 84, 314–322. https://doi.org/10.1016/j.atmosenv.2013.11.055.
Sarwar, G., Luecken, D., Yarwood, G., Whitten, G.Z., Carter, W.P.L., 2008. Impact of an updated carbon bond mechanism on predictions from the CMAQ modeling system: preliminary assessment. J Appl Meteorol Clim 47, 3–14. https://doi.org/10.1175/2007jamc1393.1.
Sarwar, G., Appel, K.W., Carlton, A.G., Mathur, R., Schere, K., Zhang, R., Majeed, M.A., 2011. Impact of a new condensed toluene mechanism on air quality model predictions in the US. Geosci. Model Dev. (GMD) 4, 183–193. https://doi.org/10.5194/gmd-4-183-2011.
Schulzweida, U., 2018. Climate Data Operators User Guide Version 1.9.3. MPI for Meteorology.
Sharkey, T.D., Monson, R.K., 2017. Isoprene research-60 years later, the biology is still enigmatic. Plant Cell Environ. 40, 1671–1678. https://doi.org/10.1111/pce.12930.
Sindelarova, K., Granier, C., Bouarar, I., Guenther, A., Tilmes, S., Stavrakou, T., Muller, J.F., Kuhn, U., Stefani, P., Knorr, W., 2014. Global data set of biogenic VOC emissions calculated by the MEGAN model over the last 30 years. Atmos. Chem. Phys. 14, 9317–9341. https://doi.org/10.5194/acp-14-9317-2014.
Utembe, S.R., Rayner, P.J., Silver, J.D., Guerette, E.A., Fisher, J.A., Emmerson, K.M., Cope, M., Paton-Walsh, C., Griffiths, A.D., Duc, H., Monk, K., Scorgie, Y., 2018. Hot summers: effect of extreme temperatures on ozone in Sydney, Australia. Atmosphere 9https://doi.org/10.3390/atmos9120466. ARTN 466.
van Dijk, A.I.J.M., Beck, H.E., Crosbie, R.S., de Jeu, R.A.M., Liu, Y.Y., Podger, G.M., Timbal, B., Viney, N.R., 2013. The Millennium Drought in southeast Australia (2001-2009): natural and human causes and implications for water resources, ecosystems, economy, and society. Water Resour. Res. 49, 1040–1057. https://doi.org/10.1002/wrcr.20123.
Zheng, Y.Q., Unger, N., Tadic, J.M., Seco, R., Guenther, A.B., Barkley, M.P., Potosnak, M.J., Murray, L.T., Michalak, A.M., Qiu, X.M., Kim, S., Karl, T., Gu, L.H., Pallardy, S.G., 2017. Drought impacts on photosynthesis, isoprene emission and atmospheric formaldehyde in a mid-latitude forest. Atmos. Environ. 167, 190–201. https://doi.org/10.1016/j.atmosenv.2017.08.017.
Zhou, S.X., Medlyn, B., Sabate, S., Sperlich, D., Prentice, I.C., 2014. Short-term water stress impacts on stomatal, mesophyll and biochemical limitations to photosynthesis differ consistently among tree species from contrasting climates. Tree Physiol. 34, 1035–1046. https://doi.org/10.1093/treephys/tpu072.